THERMO-MECHANICAL ANALYSIS OF SIC/SIC CLADDING WITH BISON INCLUDING FUEL CREEP

Nuclear Technology Research and Development

Prepared for
U.S. Department of Energy
Nuclear Technology Research and Development Advanced Fuels Campaign

G. Singh[1], R.T. Sweet[2], B.D. Wirth[2], K.A. Terrani[1] and Y. Katoh[1]
[1]Oak Ridge National Laboratory
[2]University of Tennessee, Knoxville

September 01, 2017
M3FT-17OR020201072

ORNL/SR-2017/435

SUMMARY

This report presents the results of a parametric thermo-mechanical parametric analysis of SiC/SiC cladding performed using the BISON fuel performance code. In this analysis different steady state linear heat rates (LHR) (18kW/m, 22kW/m, 26kW/m and 30kW/m) and initial fuel rod-gap thicknesses (50µm, 65µm, 80µm and 95µm) were considered along with three different model implementation of fuel creep. These include 1) no fuel creep 2) fuel creep based on the Hagrman model and 3) fuel creep based on a modified model. The fuel rod geometries used in this analysis are representative of a generic 17 x 17 fuel rod assembly used in a Westinghouse PWR.

The results show that the LHR and initial gap thickness between the fuel and the cladding have a significant impact on the fuel rod-cladding gap closure time. The LHR was found to be the major governing parameter for the time at which gap closure occurs. For fuel operated at higher LHRs, the modeling results indicate that the initial gap thickness is the most significant factor in gap closure. Fuel creep has negligible effect on gap closure in general, although with the Hagrman creep model the gap closes a little earlier than that for either the no fuel creep or Modified creep model. Fuel creep had negligible effect on the cladding stresses prior to contact between fuel rod and cladding, but significantly influence the stresses after the contact. The predicted stresses for Modified creep model were greater than those predicted by the Hagrman creep model. Fuel creep had negligible effect on the temperature distribution in the cladding but significantly impacted the axial and radial displacement of the cladding. The Modified and Hagrman creep model did not show any significant difference in the predicted radial and axial displacement of the cladding.

CONTENTS

FIGURES

TABLES

ACRONYMS

AFC	Advanced Fuels Campaign
ATF	Accident-tolerant fuel
BWR	Boiling water reactor
CVD	Chemical vapor deposition
CVI	Chemical vapor infiltration
dpa	displacement per atom
DOE-NE	US Department of Energy Office of Nuclear Energy
GFR	Gas-cooled fast reactor
LWR	Light water reactor
MSR	Molten salt reactor
ORNL	Oak Ridge National Laboratory
PWR	Pressurized water reactor
SFR	Sodium fast reactor
SiC	Silicon Carbide
SiC/SiC	Silicon carbide fiber-reinforced silicon carbide matrix composite
VHTR	Very High Temperature Reactor

THERMO-MECHANICAL ANALYSIS OF SIC/SIC CLADDING WITH BISON INCLUDING FUEL CREEP

1. INTRODUCTION

The Fukushima Daiichi nuclear power plant accident spread safety concerns over existing nuclear reactors around the globe. In efforts to enhance the safety of nuclear power plants extensive research and development work is being conducted to improve the accident tolerance of fuel-cladding systems [1, 2]. Due to its high temperature strength, relatively higher chemical stability, reasonable fracture toughness and stability under neutron irradiation, SiC/SiC composite materials are promising candidate material for accident tolerant fuel cladding systems in light water reactors (LWR) [3, 4]. In addition to its application in LWRs, SiC/SiC composites have potential structural and insulation applications in other nuclear energy systems, such as the Very High Temperature Reactor (VHTR) [5, 6], Gas-Cooled Fast Reactor (GFR) [7], Molten Salt Reactor (MSR), sodium fast reactor (SFR), and fusion reactors [8, 9].

Within the SiC cladding concept there are several types: fully composite cladding, composite layer and a monolithic SiC or a metal layer at the inside and/or outside as layered structures. This work focusses on a fully SiC/SiC composite cladding concept with UO_2 fuel. There are several fuel concepts being studied and analyzed; however, this report is focused on the cladding performance. Therefore UO_2 fuel, for which an extensive knowledge base is available, is considered as the fuel material in this work.

Studies have been conducted focusing on evaluating the viability of SiC/SiC from different perspectives including neutronics [10-13] and high-temperature water corrosion [14-16]. Earlier studies [17, 18] showed that swelling of the cladding delayed closure of the fuel rod gap and the resulting effects of fuel rod-cladding interaction. These studies also provided insights about the relatively high fuel rod temperature (compared to fuel temperatures with traditional Zirconium alloy cladding) resulting from the decreased thermal conductivity of irradiated SiC.

Recent studies [19-21] captured the stresses that develop from differential swelling as a result of the high radial heat flux, low thermal conductivity of irradiated SiC, and the highly temperature dependent swelling of SiC. Ben-Belgacem et al. [19] presented a numerical analysis of pure SiC/SiC composite cladding. The results showed development of significant stresses over a short time, mainly due to the temperature dependent swelling of the material. The analysis showed that a considerable stress variation across the thickness of the cladding exists and the stress direction is opposite to that present in a metallic cladding. Stone et al. [21] analyzed stresses in three SiC cladding concepts (fully composite, inner composite and outer monolith, and inner monolith and outer composite) for saturated swelling conditions using an analytical model. The maximum stress occurred during the cold shutdown condition. Of the three concepts, the inner composite and outer monolith SiC showed the lowest failure probability with the properties assumed in the study. Lee et al. [20] presented an analytical model for evaluating the stress distribution in the triple layered SiC cladding (monolith inner layer, composite middle layer, and monolith outer layer) under conditions of saturated swelling. It was found that the temperature dependent swelling introduced significant tensile stresses at the inner region of the cladding. The authors also analyzed a double

layered SiC cladding with an inner composite layer and outer monolith layer. The double layered SiC cladding design showed a significantly lower failure probability compared to the triple layer design. The strain associated with this differential swelling was shown to dominate the stress profile in the cladding soon after the onset of irradiation. This profile differs widely from metallic cladding.

The current work described in this report focuses on the thermo-mechanical analysis of fully composite SiC/SiC cladding with spatially varying boundary conditions that exist in pressurized water reactors (PWRs) and, to an even greater extent, in boiling water reactors (BWRs). These conditions include parametric axial variation in linear heat rate (LHR), neutron fluence, coolant temperature and fuel creep behavior. Besides evaluating the displacement and stress distribution in the cladding, this study also investigates the mechanical interaction of the fuel rod with cladding by varying the fuel rod gap thickness and LHR, as well as the influence of the three different model implementations of fuel creep. These include: 1) no fuel creep 2) fuel creep based on the Hagrman model and 3) fuel creep based on a modified model. In this study, we have used BISON, a finite-element-based nuclear fuel performance code [22].

2. METHOD

2.1 Constitutive Model

SiC/SiC composites undergo temperature dependent swelling under irradiation. This swelling strain, denoted here as $\boldsymbol{\varepsilon}^s$, saturates early at around ~1 displacement per atom (dpa) for irradiation temperatures below about 1000°C. The magnitude of the swelling strain has inverse temperature dependence. The non-uniform temperature distribution in the cladding leads to differential swelling across the thickness of the cladding, which in term cause an increase in stresses. The material undergoes irradiation creep ($\boldsymbol{\varepsilon}^c$) under the influence of these stresses and irradiation. Thermal strain in the material is denoted as $\boldsymbol{\varepsilon}^{th}$. Besides the swelling, creep and thermal expansion/contraction, the material also undergoes elastic deformation which is accounted for by the elastic strain ($\boldsymbol{\varepsilon}^e$). Thus, the total strain is composed of the elastic strain, swelling strain, creep strain and thermal strain as shown in equation (1). The stress-strain relationship is based on Hooke's law (equation (2)). The stresses are updated for each time increment in the numerical solution through equation (3).

$$\boldsymbol{\varepsilon}^{total} = \boldsymbol{\varepsilon}^e + \boldsymbol{\varepsilon}^c + \boldsymbol{\varepsilon}^s + \boldsymbol{\varepsilon}^{th} \quad (1)$$

$$\boldsymbol{\sigma} = \mathbf{D}\boldsymbol{\varepsilon}^e \quad (2)$$

$$\Delta\boldsymbol{\sigma} = \check{\mathbf{D}}\Delta\boldsymbol{\varepsilon}^e + \Delta\mathbf{D}\boldsymbol{\varepsilon}^e \quad (3)$$

where $\mathbf{D}$ is the elastic stiffness matrix and $\check{\mathbf{D}}$ is the mean elastic stiffness matrix during the numerical solution step increment. $\mathbf{D}$ is a function of dose and temperature. The next section discusses the material properties.

2.2 Material Properties

2.2.1 Material Properties for SiC/SiC Composite

Table 1 shows the dependence of SiC/SiC composite material properties on irradiation dose and temperature, considered in this analysis.

Table 1: Dependence of SiC/SiC composite material properties of cladding on irradiation and temperature.

	Temperature dependence	Effect of Irradiation
Coefficient of thermal expansion	Dependent [23]	Negligible [23]
Creep strain (Irradiation creep compliance)	Dependent [24]	Irradiation effect phenomena [24]
Swelling strain	Dependent [25, 26]	Irradiation effect phenomena [25, 26]
Specific heat capacity	Dependent	Negligible
Thermal conductivity	Dependent, basis for modeling exists [23, 25]	Strong effect, basis for modeling exists [23, 25]
Elastic constants	Dependent, basis for modeling exists [23, 25]	Minor effect, known [25]

Swelling: CVD SiC and CVI SiC/SiC shows very similar swelling properties [27, 28]. Figure 1 shows variation of swelling with fluence for CVD SiC at various temperatures. In the analysis presented herein CVI SiC/SiC composites were assigned same swelling properties as for CVD SiC shown in Figure 1.

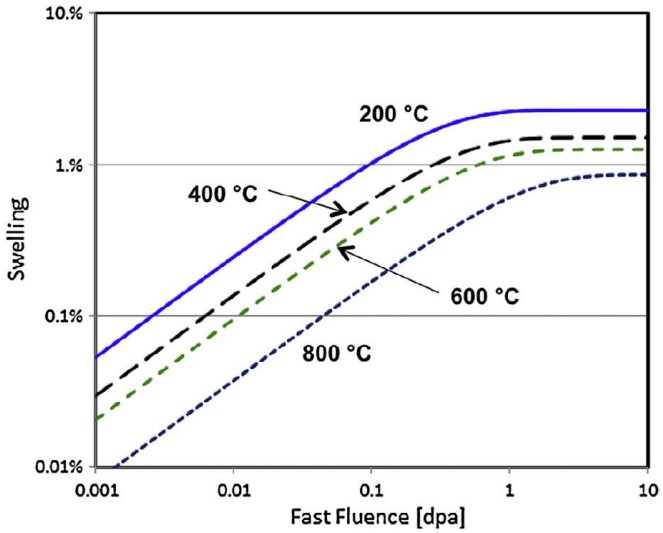

Figure 1: Swelling as a function of dose at different temperature for CVD SiC; CVI SiC/SiC was assigned same swelling properties [9].

Thermal conductivity: When SiC/SiC composites are exposed to neutron irradiation, the thermal conductivity decreases steeply and reaches saturation within a few dpa of fast neutron fluence. The net thermal resistivity (reciprocal thermal conductivity) can be expressed as a sum of thermal resistivity of the unirradiated material and increment in the thermal resistivity due to created defects [29].

$$K_{irr}^{-1} = K_{o}^{-1} + K_{rd}^{-1} \qquad (4)$$

K_{irr}^{-1}: Thermal resistivity of irradiated material
K_{o}^{-1}: Thermal resistivity of unirradiated material

K_{rd}^{-1}: Radiation defect thermal resistivity

A detailed discussion on the properties of SiC/SiC considered in the analysis are presented in reference [30].

2.2.2 Material Properties for UO_2 Fuel

The reference sources for UO_2 fuel properties employed in the analysis are provided in Table 2.

Table 2: Material Properties for UO2

Material Properties	Model	Reference
Thermal Conductivity	NFIR	[31, 32]
Specific Heat Capacity	Fink	[33]
Solid Fission Product Swelling	MATPRO	[34]
Gaseous Fission Product Swelling	MATPRO	[34]
Thermal and Irradiation Creep	MATPRO	[34]
Fission Gas Release	SIFGRS	[35]
Elastic Modulus	MATPRO	
Poisson's Ratio	Constant (0.35)	
Thermal Expansion Coefficient	MATPRO	
Relocation	ESCORE	[36]
Densification	ESCORE	[37]

These values are based on data from reference [34] and conservatively estimate the corresponding properties.

The fuel creep model proposed by Hagrman et al. [34] describes the thermal and irradiation induced creep in UO_2 using the equation 5. In this model, the total creep is expressed as a sum of fission-enhanced thermal creep (first term), thermal creep (second term) and fission-induced creep (third term). A_x are the constants, Q_x are the activation energies (J/mol), $\dot{F}$ is the fission rate (fissions/m^3·s), σ is the stress (Pa), k is the Boltzmann constant (eV/K), T is temperature (K), D is theoretical density of fuel (%) and G is the grain size (μm).

$$\dot{\varepsilon}_{total}^{fuel} = \frac{A_1 + A_2\dot{F}}{(A_3 + D)G^2}\sigma e^{\left(\frac{-Q_1}{kT}\right)} + \frac{A_4}{(A_6 + D)}\sigma^{4.5}e^{\left(\frac{-Q_2}{kT}\right)} + A_7\dot{F}\sigma e^{\left(\frac{-Q_3}{kT}\right)} \quad (5)$$

Although fuel stoichiometry can affect the activation energies, the current analysis considers considers only the oxide-to-metal ratio of 2. In this analysis the grain size has been considered to be constant 10μm. The fission-induced creep is considered to be temperature independent for lower temperature [38, 39], however, the experimental data are not consistent [40]. Solomon et al. [39] consolidated the experimental results of Perrin et al. [41] and using the Bohaboy et al. model [42] arrived at the equation 6 which did not have the temperature dependent exponential factor in the fission-induced creep term. This fuel creep model expressed in equation 6 is referred as the Modified Creep model in the document henceforth.

$$\dot{\varepsilon}_{\text{total}}^{\text{fuel}} = \frac{A_1 + A_2\dot{F}}{(A_3 + D)G^2}\sigma e^{\left(\frac{-Q_1}{kT}\right)} + \frac{A_4}{(A_6 + D)}\sigma^{4.5} e^{\left(\frac{-Q_2}{kT}\right)} + A_8\dot{F}\sigma \quad (6)$$

Table 2 shows the values of these model parameters used in the analysis presented herein.

Table 2. Constants for the fuel creep [43] [44] and modified fission-induced creep [39]

Parameter	Value	Units
A_1	0.3919	μm^2-Pa^{-1}-s^{-1}
A_2	1.31 x 10^{-19}	μm^2-m^3-Pa^{-1}
A_3	-87.7	dimensionless
A_4	2.0391 x 10^{-25}	$Pa^{-4.5}$-s^{-1}
A_6	-90.5	dimensionless
A_7	3.72264 x 10^{-35}	m^3-Pa^{-1}
A_8	1.49977 x 10^{-36}	m^3-Pa^{-1}
Q_1	3.903	eV
Q_2	5.725	eV
Q_3	0.225	eV

Considering the uncertainty in literature regarding the temperature dependence of the fission-induced creep of UO_2, the analysis has been performed with both the models: Hagrman model which has temperature dependent fission-induced creep, and modified creep model which does not include temperature dependence of fission-induced creep. In order to understand the influence of fuel creep on cladding stresses, analysis has been also performed without considering creep in the fuel model.

2.3 Modeling and Analysis

A parametric analysis was performed to identify the effects that initial fuel rod gap thickness, LHR and fuel creep model have on the gap closure behavior and cladding stress development. The analysis was performed using an axisymmetric FE model of the fuel rod and cladding. Fuel is modeled as smeared pellets. The values used for these parameters are shown in Table 3. The LHR shown in the table are rod average LHR. The local LHR in the fuel rod is a product of rod average LHR and the axial power profile peaking factor. This analysis was performed using the fuel performance code BISON [22].

Table 3: Parameters considered in the analysis.

Linear heat rates (kW/m)	Initial gap (μm)	Fuel creep model
18	50	No creep
22	65	Hagrman model
26	80	Modified model
30	95	

A section of the fuel rod and cladding mesh geometry used in the parametric analysis is shown in Figure 2. The geometric dimensions for the model were representative of a generic 17 x 17 fuel assembly from a Westinghouse PWR and are shown in Table 4. Second order quadrilateral elements with 8 nodes were used to generate the mesh of the fuel rod and cladding. The cladding was meshed with 5 elements in the radial

direction and 900 elements in the axial direction. Fuel rod was meshed with 11 elements in the radial direction and 1200 elements in the axial direction.

Table 4: Dimensions of the fuel-rod and cladding considered in the analysis.

Geometry	Dimension
Cladding outer radius	4.75 mm
Cladding wall thickness	572 μm
Cladding height	4.0 m
Fuel rod stack height	3.658 m
Top plenum gap height	0.232 m
Bottom plenum gap height	0.105 m

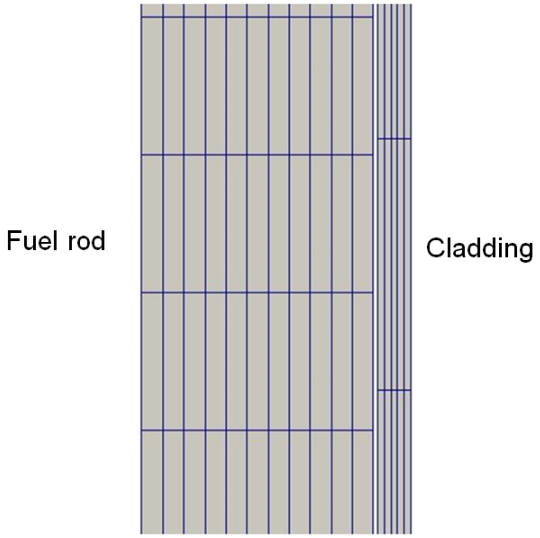

Figure 2: A section of the axisymmetric finite element model of fuel rod and cladding.

The initial plenum pressure was set to 2 MPa. An external pressure of 15 MPa, generated due to pressurized coolant, was applied at the external surface of the cladding. A thermal boundary condition for convection was applied at the cladding external surface. These boundary conditions can be expressed as:

$$k\nabla T = \mathbf{q} = h(T - T_c) \qquad (7)$$

where k, T q, h, and T_c represent thermal conductivity, temperature, heat flux, convective heat transfer coefficient, and bulk coolant temperature, respectively. The convective heat transfer coefficient is assumed to be 30 kW/m^2K.

Figure 3 shows the axial power profile applied to the fuel considered in these analyses. This profile is expressed as the ratio of local power at a given axial location to the fuel rod average power. Only 'Frictionless' mechanical contact was considered in these analyses.

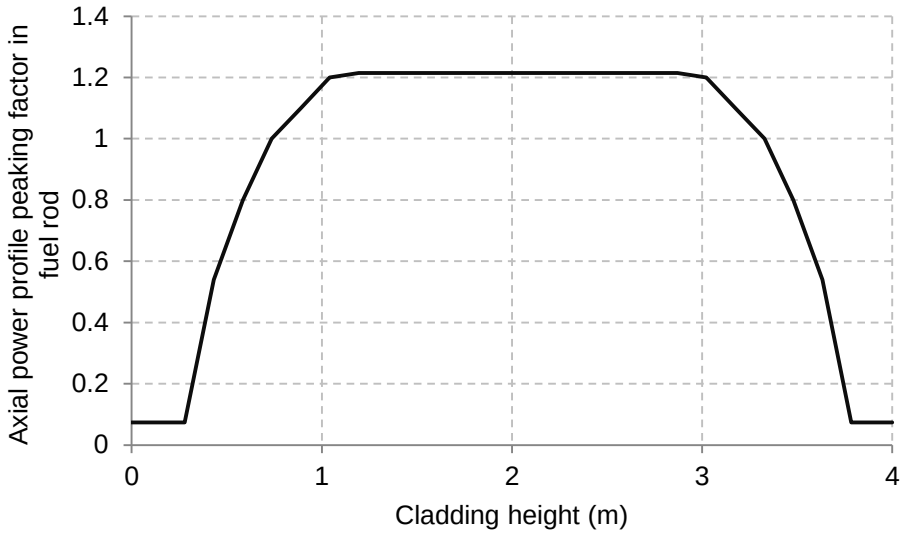

Figure 3: Axial power profile peaking factor in fuel rod considered in the analysis.

3. RESULTS

3.1 Gap Closure – Dependence on Linear Heat Rate, Initial Gap Thickness and Fuel Creep

Parametric analysis was performed using BISON for different steady state LHR (18kW/m, 22kW/m, 26kW/m and 30kW/m) and initial gap thicknesses (50µm, 65µm, 80µm and 95µm). The fuel creep had little effect on the variation of gap thickness with burnup (see Figure 4). Figure 5 shows the burnup level and reactor operation time at gap closure for each LHR and initial gap thickness considered in the analysis. A few conclusions can be drawn from the results shown in Figure 5: 1) a larger initial fuel rod-cladding gap closes after a greater burnup 2) gap closure is significantly delayed for lower LHR and 3) fuel creep slightly expedites the gap closure.

Figure 4 shows the gap thickness as a function of burnup for the different models of fuel creep. The gap closes slightly earlier using Hagrman creep model compared to that with Modified creep model or without creep. It can be noted from Figure 4 that there is a significant decrease in the fuel rod–cladding gap at the startup of the reactor. This decrease in the gap is caused by the much greater thermal expansion of the fuel compared to that of cladding. An increase in the gap thickness after the initial decrease in the gap is due to the swelling of SiC/SiC cladding under neutron irradiation as shown previously [19], and fuel densification. When the swelling in the cladding becomes saturated (~ 1 dpa) the fuel rod-cladding gap decreases at a constant rate due to fuel relocation and swelling (steady-state swelling due to fission products).

It can be noted from Figure 5 that for higher LHR the slope of the burnup/time at gap closure vs. initial gap thickness curve is greater; indicating that at higher LHR the increase in gap thickness is more effective in delaying the gap closure compared to that at lower LHR.

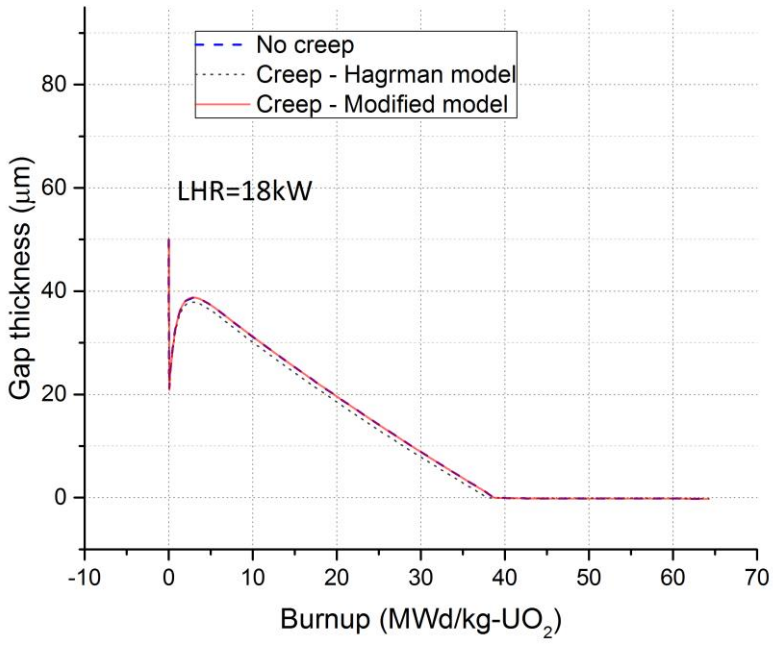

Figure 4: Gap thickness as a function of burnup for a steady-state linear heat rate of 18kW/m and initial gap thickness of 50μm.

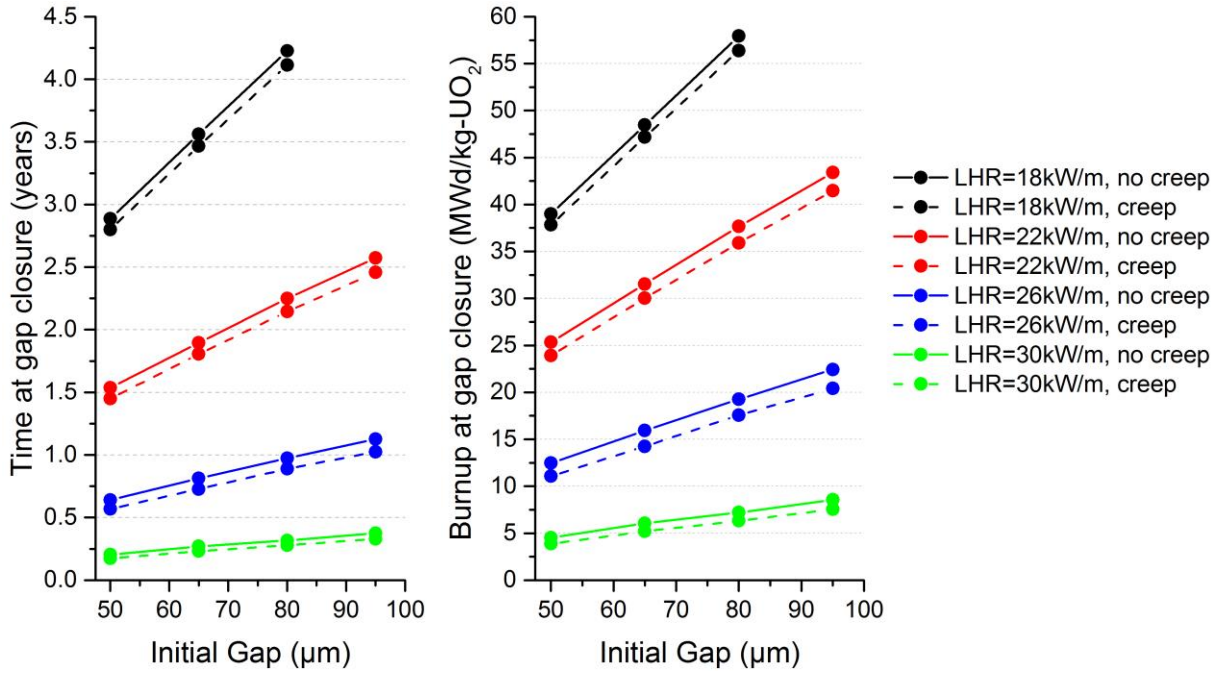

Figure 5: Burnup and time at gap closure vs. initial gap thicknesses for different LHRs and cases of fuel with and without creep. 'creep' in figure legend refers to Hagrman creep model.

3.2 Stress Temperature Distribution and Displacement of Cladding

3.2.1 Variation of Stresses and Temperature with Time

This section discusses the stress distribution and its variation in the cladding. These results were obtained from 2D axisymmetric models. Figures 6 – 8 show the hoop stresses, axial stresses and temperature in the cladding, respectively, as a function of time at the axial mid-plane of the cladding. Results are shown at the inner and outer cladding surfaces for three different cases of fuel creep: 1) no fuel creep 2) Hagrman fuel creep model and 3) Modified fuel creep model. The case with no fuel creep is incorporated in the analysis to understand the contribution of fuel creep to stress relaxation in the cladding.

As shown in Figure 6, both hoop and axial stresses are compressive at reactor startup because of the external pressure of 15 MPa in the PWR coolant. Due to the inner region of the cladding being at a higher temperature than the outer region, the inner region undergoes greater thermal expansion than the outer region. The outer region, which experiences less expansion, prevents the inner region from expanding. Thus, the inner region of the cladding is under higher compressive stresses relative to the outer region of the cladding.

SiC/SiC composite material experiences volumetric expansion due to neutron irradiation, and this swelling is inversely related to the temperature: swelling is smaller at higher temperature. Initially, when the thermal expansion of the cladding is greater than the swelling due to irradiation, the inner region of the cladding experiences greater compressive stresses than the outer region. Later, after about couple of weeks, the swelling becomes dominant cause of expansion of the cladding compared to the thermal expansion. This variation leads to higher compressive stresses in the outer region of the cladding relative to the inner region. Due to continuous release of fission gas, the rod internal pressure rises which leads to rise in the stress level even after irradiation induced swelling of the SiC cladding saturates. Since fission gas is released at a faster rate for higher LHR the stresses rise more rapidly for higher LHR.

A sudden rise in the hoop stresses of about 100 MPa for Modified creep model and about 60 MPa for Hagrman creep model can be noted in Figures 6a, 6c and 6d after about 3, 0.5 and 1 year, respectively. This rise in hoop stress is because of the contact between the cladding and the fuel rod. Figure 7 shows that the axial stresses do not show a similar rise because the ‘Frictionless’ contact model allows the fuel rod to slide freely with respect to the cladding in the axial direction without generating any additional axial stresses in the cladding. The hoop stresses for the case with a LHR of 18 kW/m and initial gap thickness of 80μm do not show a rapid rise in the stresses because fuel rod-cladding contact does not occur for this case. Figure 8 shows that the fuel creep had negligible effect on the temperature of the cladding, especially before 2 year. After 2 years, the simulation without fuel creep predicts a slightly higher temperature compared to those with fuel creep.

Figure 7 shows the variation of axial stresses at the axial mid-plane of the cladding as a function of time. There is no significant difference in the stresses for the three cases of fuel creep.

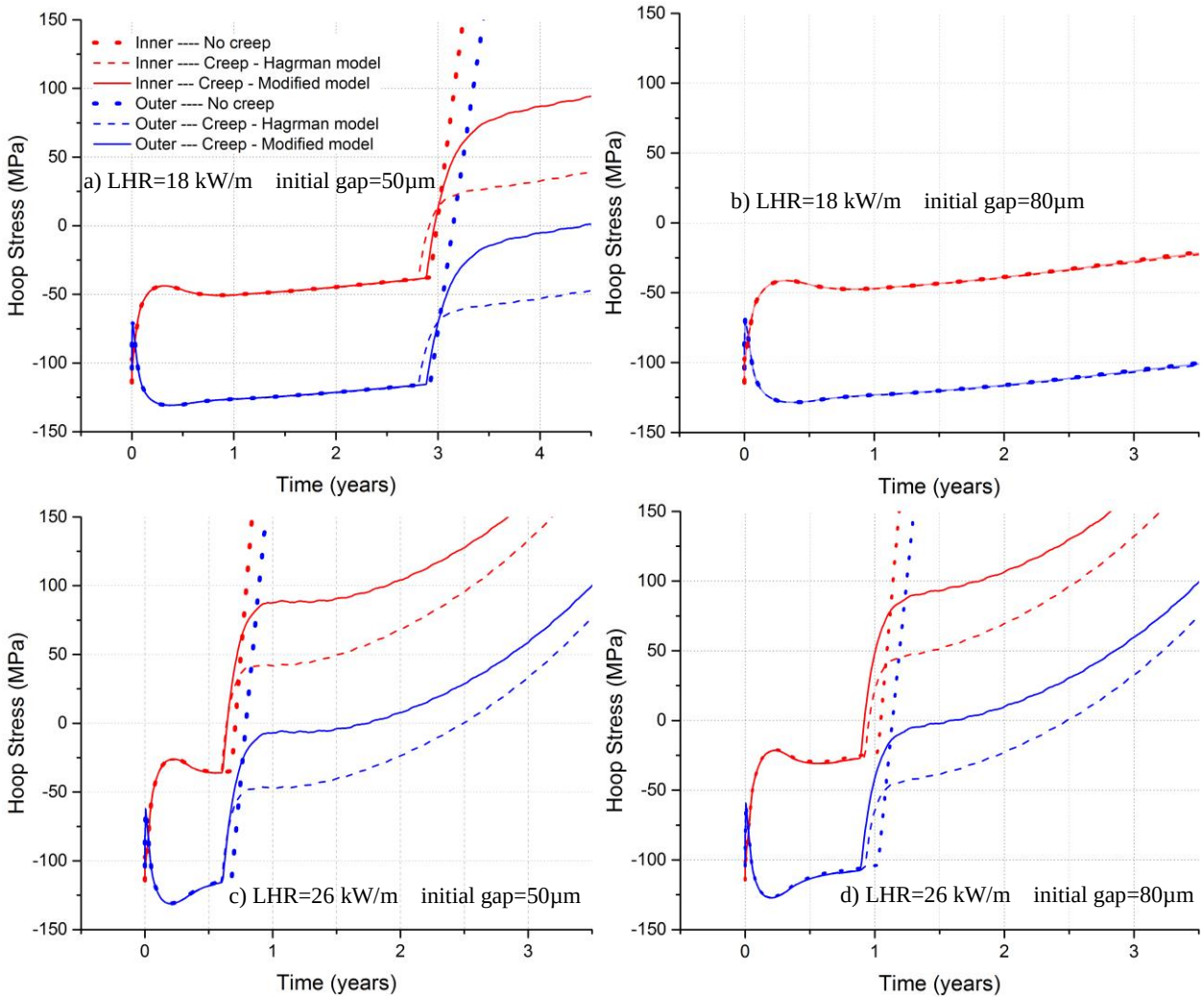

Figure 6: Variation of the hoop stress at the inner and outer cladding surfaces at the axial mid-plane of the cladding as a function of time for different cases of fuel creep.

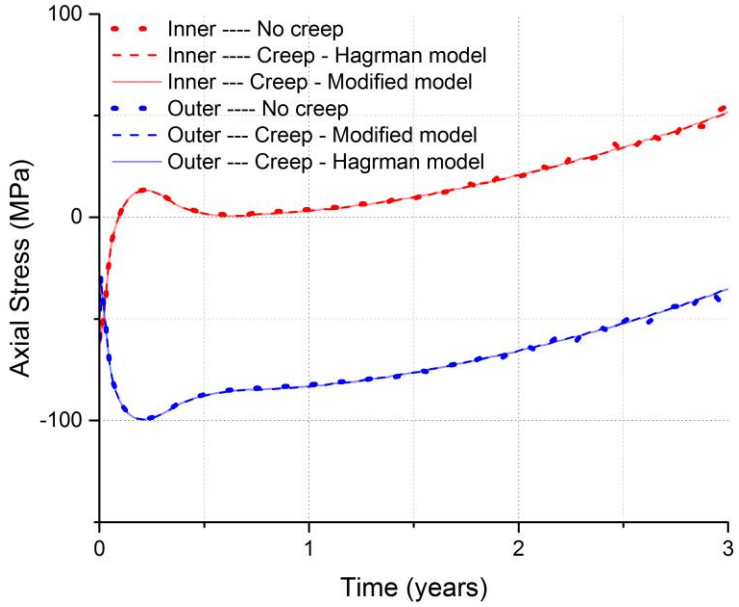

Figure 7: Variation of the axial stress at the inner and outer cladding surfaces at the axial mid-plane of the cladding as a function of time (LHR=26kW/m, initial gap thickness=80µm).

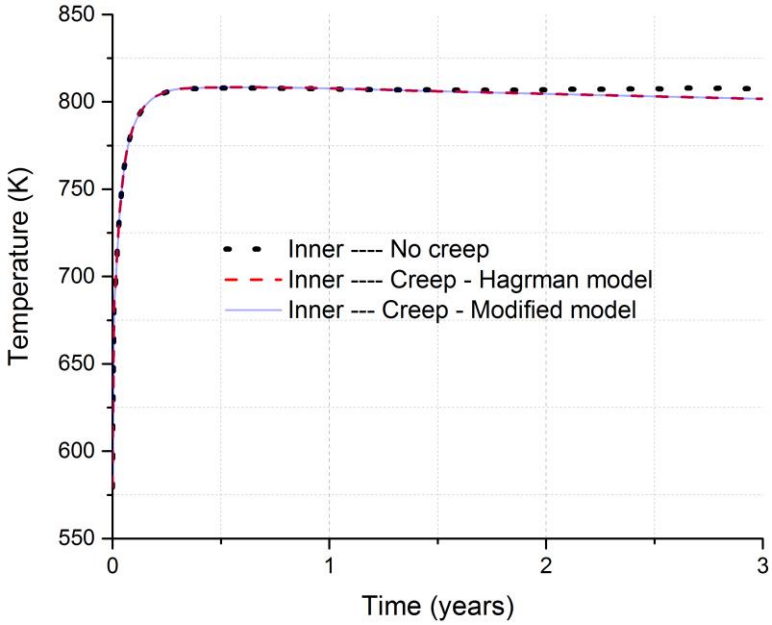

Figure 8: Variation of the temperature at the inner cladding surface at the axial mid-plane of the cladding as a function of time (LHR=26kW/m, initial gap thickness=80µm).

3.2.2 Radial and Axial Displacements in Cladding

Figure 9 shows the maximum radial and axial displacement of the cladding as a function of time. The radial displacements of the cladding for the three cases of fuel creep are same until contact occurs between the cladding and the fuel rod. After contact the cladding with no creep in the fuel rod shows significantly greater radial displacement compared to the displacements shown by the cladding with fuel creep enabled. There is no significant difference between the radial displacements of the claddings with Hagrman creep model and Modified creep model. Axial displacement also shows a similar trend as found

for radial displacement except that the axial displacement for cladding with no fuel creep is smaller than those found for the claddings with fuel creep. There is negligible difference between the axial displacements of the claddings with the Hagrman creep model and the Modified creep model.

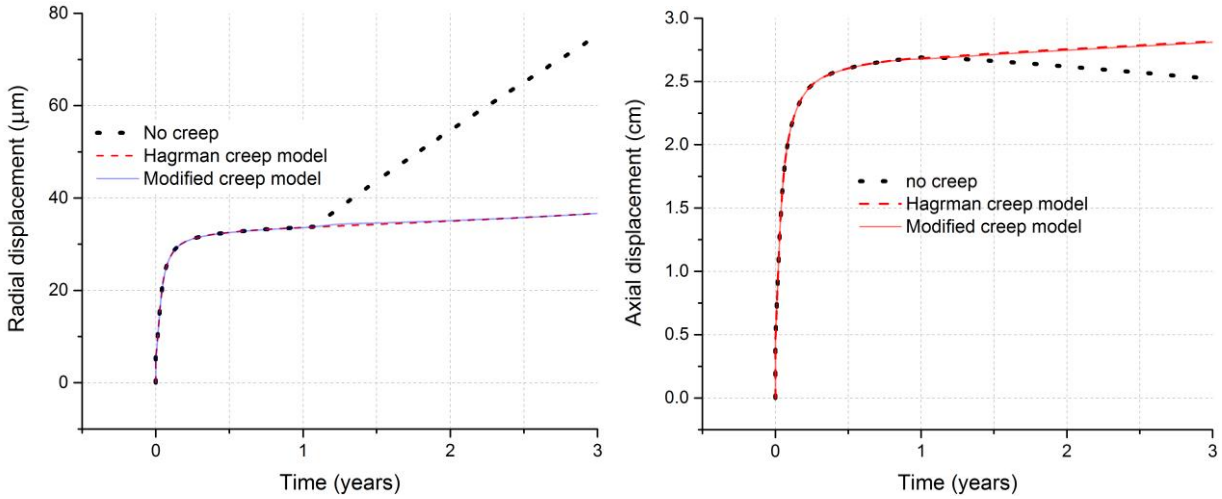

Figure 9: Variation of maximum radial displacement and axial displacement of the cladding with time (LHR=26kW/m, initial gap thickness=80μm).

3.2.3 Distribution of Stresses and Temperature along Cladding Height

Figure 10 and 11 show the distribution of hoop and axial stresses along the height of the cladding (LHR = 26kW/m and initial gap thickness = 80μm) at the end of 2 years. The H1 and H2 labels indicate the regions of beginning and end of the contact between the cladding and fuel rod. In the region where fuel rod is not in contact with the cladding, stresses in the cladding are very similar in magnitude for the cases with creep and without creep. However, in the region of fuel rod-cladding contact there is significant difference: for the case of no fuel creep, the stresses at the inner surface are much higher than those with fuel creep. The simulation with Modified creep model predicts stresses which are about 30 MPa greater than those predicted with Hagrman creep model. At the outer surface, Modified creep model predicts tensile stresses while Hagrman creep model predicts compressive stresses.

Figure 12 shows the corresponding variation in the cladding temperature at the inner and outer surface as a function of cladding height at the end of 2 years of irradiation. The figure shows that the effect of fuel creep on the cladding temperature is very small.

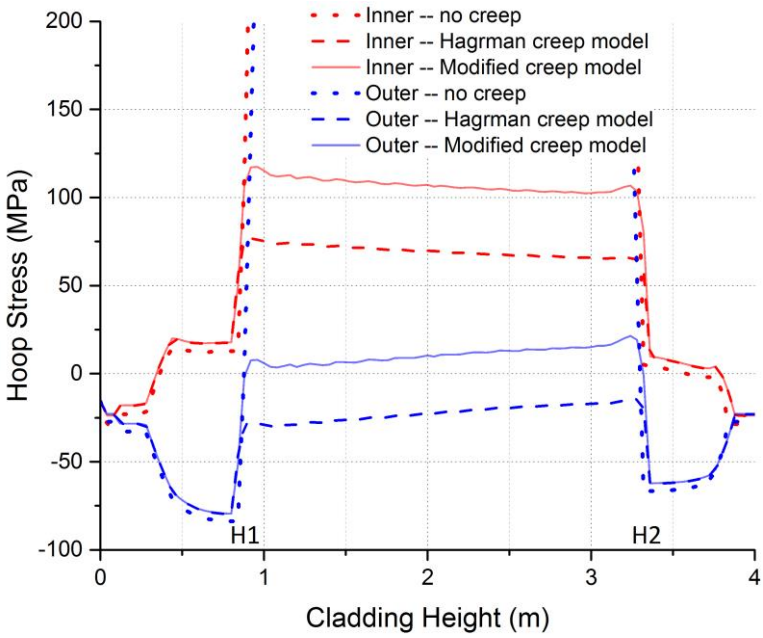

Figure 10: Variation of hoop stress along the height of the cladding (LHR = 26kW/m and initial gap thickness = 80µm) at the end of 2 years for the inner and outer cladding surfaces for different fuel creep models. H1 and H2 indicate the beginning and end of fuel rod-cladding contact.

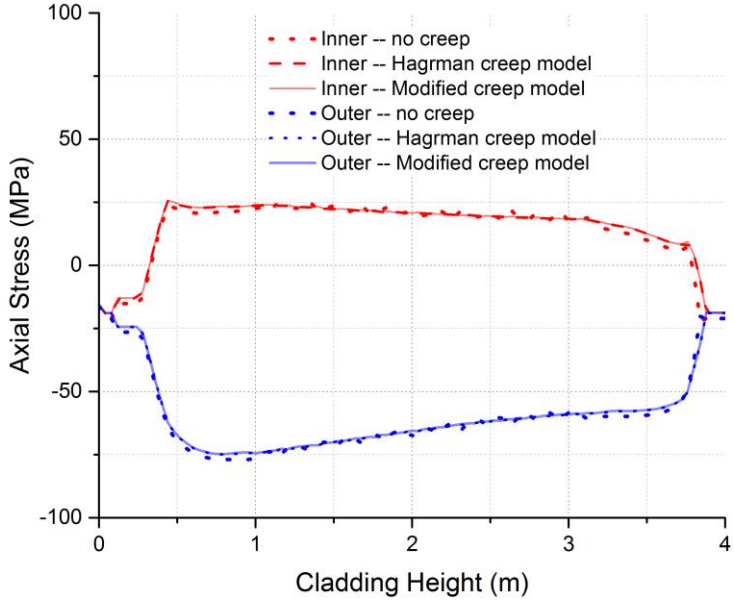

Figure 11: Variation of axial stress along the height of the cladding at the end of 2 years for the inner and outer cladding surfaces for different fuel creep models (LHR=26kW/m, initial gap thickness=80µm).

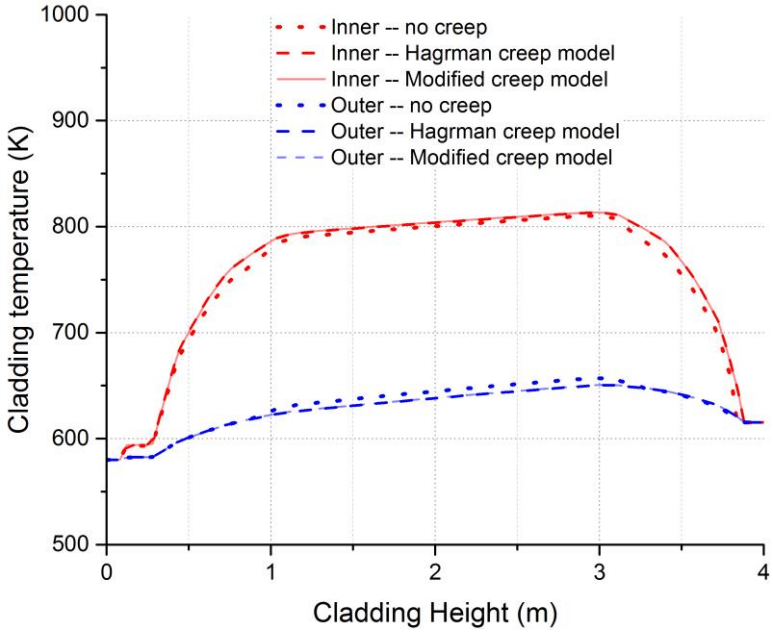

Figure 12: Variation of temperature along the height of the cladding for different fuel creep models at the end of 2 years (LHR=26kW/m, initial gap thickness=80μm).

4. CONCLUSIONS

Thermo-mechanical parametric analysis of SiC/SiC cladding was performed using the BISON fuel performance code. The analysis was performed considering three different cases of fuel creep: 1) Hagrman creep model 2) Modified creep model and 3) fuel with no creep. The results show that the LHR and initial gap thickness between the fuel and cladding have a significant impact on the fuel rod-cladding gap closure time. LHR seems to be the major governing parameter which determines the time for fuel rod-cladding gap closure. It was also found that for lower LHR the effect of initial gap thickness on gap closure is greater.

It was found that fuel creep has negligible effect on gap closure in general, although for Hagrman creep model the gap closes little earlier than for no creep and Modified creep model. The fuel creep had negligible effect on the cladding stresses prior to the contact between fuel rod and cladding. However, fuel creep significantly affected the stresses after the contact. The predicted stresses for Modified creep model were greater than those predicted by the Hagrman creep model. Fuel creep had negligible effect on the temperature distribution in the cladding but significantly impacted the axial and radial displacement of the cladding. The Modified creep model and Hagrman creep model did not predict any significant differences in the radial and axial displacement.

Specific fuel geometries known to cause PCI failures (e.g., discrete fuel cracks and missing pellet surface defects) have not yet been analyzed for SiC/SiC cladding. These topics will be the focus of forthcoming work on thermo-mechanical analysis of SiC/SiC cladding.

ACKNOWLEDGMENTS

The authors would like to thank the BISON (Ben Spencer and Stephen Novascone) and MOOSE (Cody Permann and Derek Gaston) code developers for their technical support for this work**.** This research made use of the resources of the High Performance Computing Center at Idaho National Laboratory, which is supported by the Office of Nuclear Energy of the U.S. Department of Energy and the Nuclear Science User Facilities under Contract No. DE-AC07-05ID14517. This research is sponsored by the Advanced Fuels Campaign of the Nuclear Technology Research and Development program, Office of Nuclear Energy, US Department of Energy, under contract DE-AC05-00OR22725 with UT-Battelle, LLC.

5. REFERENCES

1. Carmack, J., et al. *Overview of the US DOE accident tolerant fuel development program*. in *Proc. 2013 LWR Fuel Performance Meeting/TopFuel 2013*. 2013.
2. Zinkle, S.J., et al., *Accident tolerant fuels for LWRs: A perspective.* Journal of Nuclear Materials, 2014. **448**: p. 374-379.
3. Yueh, K., D. Carpenter, and H. Feinroth, *Clad in clay.* Nuclear Engineering International, 2010. **55**(666): p. 14-16.
4. Yueh, K. and K.A. Terrani, *Silicon carbide composite for light water reactor fuel assembly applications.* Journal of Nuclear Materials, 2014. **448**: p. 380-388.
5. Barrett, K.E., et al., *Engineering challenges of LWR advanced fuel cladding technology in preparation for in-reactor demonstrations*. 2012, Oak Ridge National Laboratory (ORNL).
6. Fazluddin, S., K. Smit, and J. Slabber. *The use of advanced materials in VHTR's*. in *Second International Topical Meeting on High Temperature Reactor Technology*. 2004.
7. Kohyama, A., et al. *R& D of Advanced material systems for reactor core component of gas cooled fast reactor*. in *Proceedings of the International Congress on Advances in Nuclear Power Plants*. 2005.
8. Raffray, A., et al., *Design and material issues for high performance SiC f/SiC-based fusion power cores.* Fusion Engineering and Design, 2001. **55**(1): p. 55-95.
9. Morley, N.B., et al., *Recent research and development for the dual-coolant blanket concept in the US.* Fusion Engineering and Design, 2008. **83**(7): p. 920-927.
10. Bloore, D.A., *Reactor physics assessment of thick silicon carbide clad PWR fuels*. 2013, Massachusetts Institute of Technology.
11. George, N.M., et al., *Neutronic analysis of candidate accident-tolerant cladding concepts in pressurized water reactors.* Annals of Nuclear Energy, 2015. **75**: p. 703-712.
12. Brown, N.R., et al., *Neutronic evaluation of a PWR with fully ceramic microencapsulated fuel. Part I: Lattice benchmarking, cycle length, and reactivity coefficients.* Annals of Nuclear Energy, 2013. **62**: p. 538-547.
13. Brown, N.R., M. Todosow, and A. Cuadra, *Screening of advanced cladding materials and UN–U 3 Si 5 fuel.* Journal of Nuclear Materials, 2015. **462**: p. 26-42.
14. Terrani, K.A., et al., *Hydrothermal corrosion of SiC in LWR coolant environments in the absence of irradiation.* Journal of Nuclear Materials, 2015. **465**: p. 488-498.
15. Kondo, S., et al., *Effect of Irradiation Damage on Hydrothermal Corrosion of SiC.* Journal of Nuclear Materials, 2015. **464**: p. 36-42.
16. Kim, D., et al., *Effect of dissolved hydrogen on the corrosion behavior of chemically vapor deposited SiC in a simulated pressurized water reactor environment.* Corrosion Science 2015. **98**: p. 304–309.
17. *Falcon-Based Comparative Assessment of Prototype Zr-4 and SiC Fuel Rod, EPRI-1022907*. 2011, Electric Power Research Institute, Palo Alto, CA.
18. Carpenter, D.M., *An assessment of silicon carbide as a cladding material for light water reactors*. 2010, Massachusetts Institute of Technology.
19. Ben-Belgacem, M., et al., *Thermo-mechanical analysis of LWR SiC/SiC composite cladding.* Journal of Nuclear Materials, 2014. **447**(1-3): p. 125-142.
20. Lee, Y. and M.S. Kazimi, *A structural model for multi-layered ceramic cylinders and its application to silicon carbide cladding of light water reactor fuel.* Journal of Nuclear Materials, 2015. **458**: p. 87-105.
21. Stone, J., et al., *Stress analysis and probabilistic assessment of multi-layer SiC-based accident tolerant nuclear fuel cladding.* Journal of Nuclear Materials, 2015.

22. Williamson, R., et al., *Multidimensional multiphysics simulation of nuclear fuel behavior.* Journal of Nuclear Materials, 2012. **423**(1): p. 149-163.
23. Katoh, Y., et al., *Continuous SiC fiber, CVI SiC matrix composites for nuclear applications: Properties and irradiation effects.* Journal of Nuclear Materials, 2014. **448**: p. 448-476.
24. Katoh, Y., et al., *Observation and possible mechanism of irradiation induced creep in ceramics.* Journal of Nuclear Materials, 2013. **434**(1): p. 141-151.
25. Snead, L.L., et al., *Handbook of SiC properties for fuel performance modeling.* Journal of Nuclear Materials, 2007. **371**(1-3): p. 329-377.
26. Katoh, Y., et al., *Stability of SiC and its composites at high neutron fluence.* Journal of Nuclear Materials, 2011. **417**(1-3): p. 400-405.
27. Hegeman, J., et al., *Mechanical and thermal properties of SiC f/SiC composites irradiated with neutrons at high temperatures.* Fusion engineering and design, 2005. **75**: p. 789-793.
28. Katoh, Y., *Final Report on Irradiation of Bonded-fiber SiC Composite, ORNL/TM-2012/201, Oak Ridge National Laboratory.* 2010.
29. Snead, L., S. Zinkle, and D. White, *Thermal conductivity degradation of ceramic materials due to low temperature, low dose neutron irradiation.* Journal of nuclear materials, 2005. **340**(2): p. 187-202.
30. Singh, G., K.A. Terrani, and Y. Katoh, *3D Thermo-Mechanical Assessment of SiC/SiC Composite Cladding for LWR Applications.* Journal of nuclear materials, 2017.
31. Marion, A., *letter dated June 13, 2006 to HN Berkow (USNRC/NRR). Safety Evaluation by the Office of Nuclear Reactor Regulation of Electric Power Research Institute (EPRI) Topical Report TR-1002865, Topical Report on Reactivity Initiated Accidents: Bases for RIA Fuel rod Failures and Core Coolability Criteria*. 2006.
32. *Response to Requests for Additional Information (RAI's) NRR Safety Evaluation Report – Project No. 689, Appendix C-1.A, pp C-1-15-16.* .
33. Fink, J., *Thermophysical properties of uranium dioxide.* Journal of nuclear materials, 2000. **279**(1): p. 1-18.
34. Hagrman, D., C. Allison, and G. Berna, *SCDAP/RELAP5/MOD 3.1 code manual: MATPRO, A library of materials properties for Light-Water-Reactor accident analysis. Volume 4*. 1995, Nuclear Regulatory Commission, Washington, DC (United States). Div. of Systems Technology; Lockheed Idaho Technologies Co., Idaho Falls, ID (United States).
35. Pastore, G., et al., *Physics-based modelling of fission gas swelling and release in UO 2 applied to integral fuel rod analysis.* Nuclear Engineering and Design, 2013. **256**: p. 75-86.
36. Kramman, M. and H. Freeburn, *ESCORE-the EPRI Steady-State Core Reload Evaluator Code: General Description.* EPRI NP-5100, EPRI, Palo Alto, California, 1987.
37. Rashid, Y., R. Dunham, and R. Montgomery, *Fuel analysis and licensing code: FALCON MOD01*. EPRI Report, 2004. **1011308**.
38. Solomon, A., *Radiation-Induced Creep of UO2.* Journal of the American Ceramic Society, 1973. **56**(3): p. 164-171.
39. Solomon, A.A., J.L. Routbort, and J.C. Voglewede, *Fission-Induced Creep of UO2 and Its Significance to Fuel-Element Performance.* 1971, Argonne National Lab., Argonne, Illinois
40. Dienst, W., *Irradiation induced creep of ceramic nuclear fuels.* Journal of Nuclear Materials, 1977. **65**: p. 1-8.
41. Perrin, J., *Irradiation-induced creep of uranium dioxide.* Journal of Nuclear Materials, 1971. **39**(2): p. 175-182.
42. Bohaboy, P., R. Asamoto, and A. Conti, *COMPRESSIVE CREEP CHARACTERISTICS OF STOICHIOMETRIC URANIUM DIOXIDE*. 1969, General Electric Co., Sunnyvale, Calif. Breeder Reactor Development Operation.

43. Hagrman, D.T., C.M. Allison, and G.A. Berna, *SCDAP/RELAP5/MOD 3.1 code manual: MATPRO, A library of materials properties for Light-Water-Reactor accident analysis. Volume 4*. 1995.
44. Hales, J., et al., *BISON theory manual: The equations behind nuclear fuel analysis*. 2014, Fuels Modeling & Simulation Department, Idaho National Laboratory, Idaho Falls, Idaho.